Search for orbital moments in underdoped cuprate metals

S.-H. Lee
University of Maryland, College Park, Maryland 20742
and NIST Center for Neutron Research, National Institute of Standards and Technology, Gaithersburg, Maryland 20899

C. F. Majkrzak
NIST Center for Neutron Research, National Institute of Standards and Technology, Gaithersburg, Maryland 20899

S. K. Sinha
Advanced Photon Source, Argonne National Laboratories, Argonne, Illinois 60439

C. Stassis
Department of Physics and Ames Laboratory, Iowa State University, Ames, Iowa 50011

H. Kawano
RIKEN, Magnetic Materials Laboratory, Hirosawa 2-1 Wako, Saitama 351-01, Japan

G. H. Lander
European Commission, Joint Research Center, Postfach 2340, D-76125 Karlsruhe, Germany

P. J. Brown
Institut-Laue-Langevin, Boîte Postale 156X, F-38042 Grenoble, France

H. F. Fong
Department of Physics, Princeton University, Princeton, New Jersey 08544

S-W. Cheong
Bell Laboratories, Lucent Technologies, Murray Hill, New Jersey 07974
and Department of Physics and Astronomy, Rutgers University, Piscataway, New Jersey 08854

H. Matsushita
Department of Physics, Tohoku University, Aramakai Aoba, Sendai 980-77, Japan

K. Yamada
Institute for Chemical Research, Kyoto University, Uji, 611-0011 Kyoto, Japan

Y. Endoh
Department of Physics, Tohoku University, Aramakai Aoba, Sendai 980-77, Japan
(Received 23 February 1999)

Polarized neutron-diffraction experiments have been performed in search of the orbital magnetic moments recently predicted in a theory for the cuprate metals. Both $La_{2-x}Sr_xCuO_4$ [LSCO(x)] and $YBa_2Cu_3O_{6+x}$ [YBCO(x)] compounds were investigated. No definitive evidence for the existence of such a three-dimensionally ordered moment was found in any of these samples within experimental uncertainty, which was as low as $0.01\mu_B$. We have also investigated the possibility that a magnetic rod exists parallel to the c axis in the case of two- or quasi-two-dimensional ordering in the (a,b) plane and have set an upper limit for the total moment to be $0.1\mu_B$ in LSCO ($x=0.1$). [S0163-1829(99)02938-0]

I. INTRODUCTION

Cuprates, which exhibit high-T_c superconductivity over a certain range of excess charge carrier doping, still pose mysteries with their rich phase diagram, including unusual metallic phases as well as the superconducting phase. Recently, the occurrence of a phase with anomalous Raman scattering, transport, and magnetic properties in underdoped cuprate metals has caused much speculation about the nature of a so-called ''pseudogap'' state[1] wherein neither long-range spin antiferromagnetism nor superconductivity occurs. Motivated by these experimental studies, a comprehensive theory for the anomalous normal state and superconductivity in cuprate metals has been presented by Varma.[2] In this theory, the cuprate metals have a continuous transition (changing to a crossover with increasing disorder) at a temperature $T_{cc}(x)$ to an unusual phase (identified with the ''pseudogap'' phase)

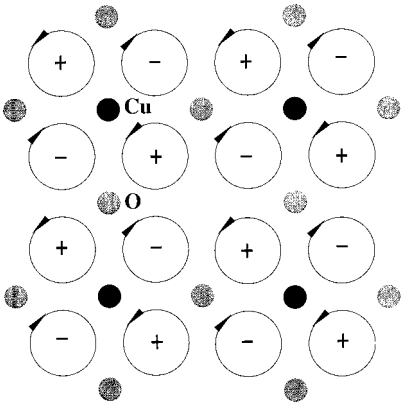

FIG. 1. The pattern of orbital moments due to circulating currents in the CuO_4 plane predicted by Varma (Ref. 2). Dark filled circles represent Cu^{2+} ions, light color circles are O^{2+}, and open circles with arrows represent the predicted circulating currents which have an antiferromagnetic order.

in which a fourfold pattern of currents circulate around each Cu atom in the CuO_2 plane. This phase is predicted to occur in the underdoped cuprates terminating in a quantum critical point $T_{cc}=0$ at $x=x_c$, the composition for optimal T_c. The predicted current pattern and the associated orbital moments (reproduced from Fig. 6 of Ref. 2) in the circulating current phase is illustrated in Fig. 1. Such moments would give rise to a magnetic neutron-diffraction pattern centered on certain Bragg points. With polarized neutron diffraction, it is possible, in principle, to observe such magnetic order. In this paper, we report polarized neutron-diffraction measurements on $La_{2-x}Sr_xCuO_4$ [LSCO(x)] ($x=0.075$, 0.10, and 0.15) and $YBa_2Cu_3O_{6+x}$ [YBCO(x)] ($x=0.5$ and 0.7) samples. In Sec. II, we briefly discuss which magnetic reflections would be allowed for possible arrangements of such moments. In Sec. III, we describe our experimental configurations and data analysis techniques. Descriptions of the LSCO ($x=0.075$, 0.10, and 0.15) and YBCO ($x=0.5$ and $x=0.7$) samples are presented in Sec. IV. The experimental results and conclusions are discussed in Secs. V and VI, respectively. Given the instrumental and sample-related limitations of these experiments, our results show no definite evidence for the existence of the predicted moment within a sensitivity of $0.01\mu_B$ for three-dimensional long-range order and $0.1\mu_B$ for two-dimensional order.

II. MODEL MAGNETIC STRUCTURE FACTORS

For such long-range ordered magnetic orbital moments as shown in Fig. 1, elastic magnetic scattering would occur at nuclear Bragg points:[3]

$$\sigma_M=\left(\frac{r_0}{2}\right)^2|f(\vec{Q})|^2\{|\vec{F}_M(\vec{Q})|^2-|\hat{Q}\cdot\vec{F}_M(\vec{Q})|^2\}\sum_{\vec{\tau}}\delta(\vec{Q}-\vec{\tau}). \quad (1)$$

Here $\vec{F}_M$ is the magnetic and the nuclear structure factor in a unit cell for the reflection of interest and $f(\vec{Q})$ is the magnetic form factor for the orbital moment corresponding to its spatial extent. r_0 is the product of the gyromagnetic ratio and classical electron radius and $\vec{\tau}$ is the magnetic reciprocal-lattice vectors which in this case are the same as the nuclear reciprocal-lattice vectors. The magnetic structure factor $\vec{F}_M$ could have different Q dependences, depending on the dimensionality of the correlations of the moments and the crystal structure. If the orbital moments, $\vec{M}=\langle\vec{\mu}\rangle=g\langle\vec{J}\rangle\mu_B$, order two-dimensionally in the CuO_2 plane, the magnetic structure factor $\vec{F}_M$ of the orbital moment configuration can be written as

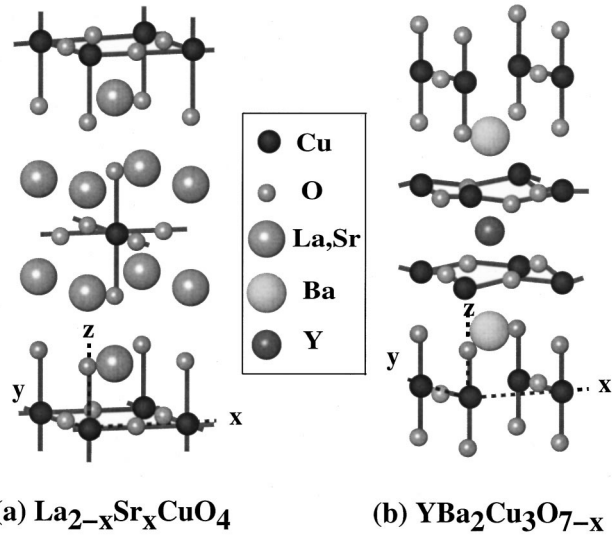

FIG. 2. Crystal structures for (a) $La_{2-x}Sr_xCuO_4$ and (b) YBCO.

$$\vec{F}_M=N\vec{M}\sin 2\pi h\beta\cdot\sin 2\pi k\beta, \quad (2)$$

where N is the number of the orbital moments in the CuO_2 plane and β is the fractional displacement of the orbital moment from the neighboring Cu ion in the lattice unit. The effect of a three-dimensional correlation of the moments depends on the crystal structure and collapses the scattered intensity from being distributed along a rod to being concentrated at a point in reciprocal space. For the case of the monolayer system LSCO (x) shown in Fig. 2(a), the result is that

$$\vec{F}_M=N\vec{M}\sin 2\pi h\beta\cdot\sin 2\pi k\beta\cdot\{1\pm\exp^{i\pi(h+k+l)}\}, \quad (3)$$

where + and − represent ferromagnetic (FM) and antiferromagnetic (AFM) interlayer couplings, respectively. Hence for nonzero intensity, $(h+k+l)$ should be even or odd, depending on whether the current pattern is the same or reversed in adjacent layers. For the bilayer system $YBa_2Cu_3O_{7-x}$ [YBCO(x)] shown in Fig. 2(b), $\vec{F}_M$ becomes

$$\vec{F}_M=N\vec{M}\sin 2\pi h\beta\cdot\sin 2\pi k\beta\cdot\{\exp^{i\pi l\Delta z}\pm\exp^{-i\pi l\Delta z}\}, \quad (4)$$

where Δz (~ 0.29 in l.u.) is the separation of the bilayers, and + and − represent FM and AFM interlayer couplings, respectively. Therefore, for FM interlayer coupling the maximum of $\vec{F}_M$ occurs at $l=0$, whereas for AFM coupling the maximum occurs at an l closest to 1.72.

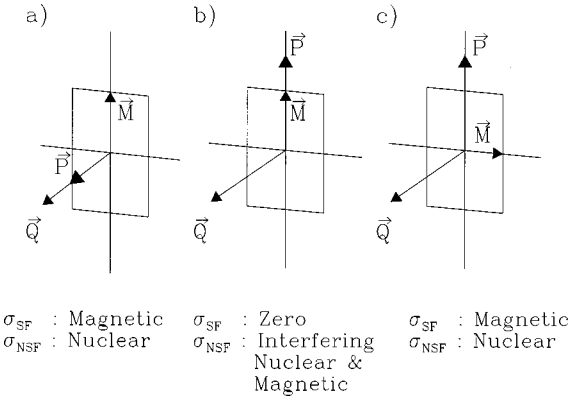

FIG. 3. Experimental geometries employed to observe the orbital moments. $\vec{M}$ is the orbital moment, $\vec{P}$ is the polarization of the incident neutrons, and $\vec{Q}$ is the wave vector of interest.

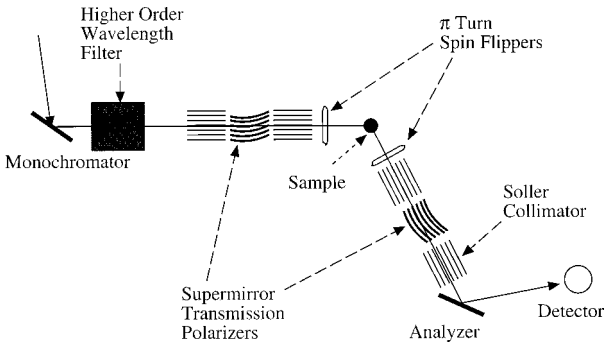

FIG. 4. A typical experimental setup for polarized neutron diffraction.

III. EXPERIMENTAL METHODOLOGY

A. Conventional polarized neutron-diffraction measurements performed at NIST

The scattering of neutrons by magnetic moments in condensed matter depends not only on the size of the moment but on the relative orientations of a triad of vectors; the neutron polarization $\vec{P}$, the moment $\vec{M}$, and the wave-vector transfer $\vec{Q}$ $(=\vec{k}_i-\vec{k}_f$, the initial and final neutron wave vectors, respectively). By measuring polarization-dependent scattered intensities for a sufficient number of Bragg reflections from a single-crystalline sample, it is possible, in principle, to determine both the absolute magnitude and spatial orientation of individual magnetic moments within a unit cell—if the directions of that triad of vectors are properly configured. Furthermore, for a significant class of structural investigations, it is necessary to consider only the component of the scattered neutron polarization along the incident direction of polarization, as described in the work of Moon *et al.*[4] Labeling one spin state of the neutron ''+'' and the other ''−,'' four spin-dependent scattering cross sections, σ_{++}, σ_{--}, σ_{+-}, and σ_{-+} (where the subscripts refer to the initial and scattered neutron spin eigenstate, respectively), can be measured if the incident neutron beam is polarized and the polarization state of the reflected neutrons is analyzed. For a collinear antiferromagnetic structure, such as that which is sought in the present study, the pair of spin-flip cross sections are equal to each other and can be referred to as σ_{SF}.

In order to establish whether the particular magnetic structure proposed in Ref. 2 does indeed exist, magnetic scattering must be observed at specific locations in reciprocal space and with the requisite strength compared to the nuclear scattering intensities arising from the known chemical structure. Given that the observable magnetic and nuclear Bragg reflections coincide for the postulated structure, it is necessary to separate the nuclear and magnetic scattering components. Appropriate experimental geometries for accomplishing this goal are illustrated in Fig. 3. Note that in general, only projections of the magnetic moment M in the plane normal to $\vec{Q}$ give rise to scattering of magnetic origin. Although the presence of disordered nuclear spins causes additional spin-dependent scattering, this scattering is incoherent and isotropic. This spin-dependent background can be measured adjacent to the Bragg peaks of interest and subtracted.

Ideally, either configuration (a) or (c) of Fig. 3 can be used to sort the magnetic and nuclear scattering into spin-flip (SF) and non-spin-flip (NSF) channels, respectively. In practice, however, a completely clean separation cannot be achieved because of the contamination of the two channels due to imperfect instrumental polarizing efficiencies. The smaller the ratio of magnetic to nuclear scattering and/or the lower the instrumental polarizing efficiencies, the more significant the corrections which must be made become.

An instrument schematic typical of the arrangements used for the experiments reported here is shown in Fig. 4. A monochromatic beam is polarized in one eigenstate by the forward transmission polarizing element (and can be subsequently rotated adiabatically to the other spin state by a π spin turn device or ''flipper'') prior to incidence on the sample. The polarization state of the beam reflected by the sample at a given scattering angle, $2\theta_s$, is analyzed with the rear flipper and polarizer combination downstream of the sample. Specific details regarding the apparatus used in this experiment are given below.

Consider now the case where $\vec{P}$ is chosen to be perpendicular to $\vec{M}$, i.e., either (a) or (c) of Fig. 3. Then σ_{NSF} is purely chemical in origin. If the instrumental efficiencies of the forward polarizer, rear polarizer, and forward flipper are defined as F, R, and f, respectively, then the NSF and SF cross sections σ_{NSF} and σ_{SF} are related to the intensities I^{off} and I^{on} measured with the front flipper in the ''off'' and ''on'' states by the following (see, for example, Ref. 5):

$$\frac{I^{\mathrm{off}}}{C}=\sigma_{\mathrm{NSF}}\frac{1+FR}{2}+\sigma_{\mathrm{SF}}\frac{1-FR}{2},$$

$$\frac{I^{\mathrm{on}}}{C}=\sigma_{\mathrm{NSF}}\frac{1+FR(1-2f)}{2}+\sigma_{\mathrm{SF}}\frac{1-FR(1-2f)}{2}, \quad (5)$$

where the factor C is a normalization constant. For perfect instrumental efficiencies, $F=R=f=1$ and $I^{\mathrm{off}}\propto\sigma_{\mathrm{NSF}}$ whereas $I^{\mathrm{on}}\propto\sigma_{\mathrm{SF}}$.

Thus two instrumental parameters need to be determined, the product of the polarizer efficiencies FR and the forward flipper efficiency f. This can be accomplished by measuring four intensities corresponding to the four possible combinations of forward and rear flipper states in either the incident beam with no sample or for a beam scattered by a sample for

which the SF cross section is identically zero (see again, e.g., Ref. 5). Note that two of the four measurements require the use of a second or rear flipper.

Nonetheless, there is no assurance that the instrumental efficiencies measured at one scattering angle of the instrument are exactly the same as those in effect at another. This is particularly problematic when the σ_{SF} of interest is orders of magnitude less than that of the corresponding σ_{NSF} and FR and f must, consequently, be determined to exceedingly high accuracy. Such is the case in the present study. It is then preferable, if not essential, to measure FR and f at an instrumental scattering angle identical to that where the SF and NSF cross sections of interest are measured so that possible systematic errors correlated with the relative positions of instrumental polarizing and flipping devices, or differing neutron flight paths, are minimized. This goal can be best realized by using the sample itself, at the same reflection of interest for the measurement of the predicted moment, as a scatterer—but in a state where either the ordered magnetic moment has vanished (above T_{cc}) or with the moment aligned parallel to the neutron polarization as shown in Fig. 3(b) so that σ_{SF} is zero.

In practice, it was determined that the efficiency f of the simple flat coil neutron polarization flipper, in every configuration used, was nearly unity (to within 0.005) and had negligible effect on instrumental corrections. On the other hand, variations of the instrumental polarizing efficiency with divergence angle and cross sectional position in the incident and reflected beams were problematical. These variations are exacerbated by larger sample crystal mosaic distributions. Of course, the smaller the size and the tighter the angular collimation of the beam, the more uniform the instrumental polarization which could be obtained, but at a corresponding loss of intensity. A compromise between polarization efficiency and intensity was made which minimized the uncertainties in the measured quantities of interest. Contrary to what might at first be expected, the performance of the supermirror transmission polarizers used, the polarizing efficiency of which are inherently angular dependent, proved to be comparable or superior to more conventional Heusler crystal polarizers (which are subject to multiple and simultaneous scattering processes that also can deleteriously effect polarizing efficiency). Another significant but related complication was encountered with the $La_{2-x}Sr_xCuO_4$ samples studied. A tetragonal-to-orthorhombic structural phase transition occurs in a temperature range close to that predicted for the appearance of the orbital moment. Associated with this structural phase transition is a change in peak shape and width in both longitudinal and transverse scan directions in reciprocal space which can potentially, and in fact do, affect the uniformity of the beam polarization. Particular attention to the instrumental and sample-related structural parameters is required to recognize the spurious effects caused by such interfering phenomena. Considerable effort was expended in optimizing flipper currents, adjusting magnetic guide fields for maximum uniformity, selecting optimum beam aperture dimensions, and establishing adiabatic guide field rotations to achieve the proper neutron polarization axis at the sample position.

From Eq. (4) above, the following expressions for σ_{NSF} and σ_{SF} are obtained:

$$\sigma_{NSF} \propto I^{off}\left[\frac{1-FR(1-2f)}{2FRf}\right]+I^{on}\left[\frac{-1+FR}{2FRf}\right],$$

$$\sigma_{SF} \propto I^{off}\left[\frac{-1-FR(1-2f)}{2FRf}\right]+I^{on}\left[\frac{1+FR}{2FRf}\right]. \qquad (6)$$

The factors in the square brackets containing the instrumental parameters FR and f can be expressed in terms of the four independent intensities, as discussed above, which were obtained for the four possible flipper state combinations with σ_{SF} equal to zero. Subsequent analysis of the corresponding statistical uncertainties in σ_{SF} and σ_{NSF} can be performed so that the final uncertainty in any measured magnetic moment can be properly evaluated. Although somewhat complicated, the determination of the necessary partial derivatives is straightforward and can be expedited using a symbolic algebra computer program.

Once σ_{NSF} and σ_{SF} have been determined for a given reflection and sample composition, the moment per orbital current loop is obtained from[3]

$$\frac{\sigma_{SF}(\vec{Q})}{\sigma_{NSF}(\vec{Q})}=\frac{(r_0/2)^2|f(\vec{Q})|^2\{|\vec{F}_M(\vec{Q})|^2-|\hat{Q}\cdot\vec{F}_M(\vec{Q})|^2\}}{|F_N(Q)|^2}, \qquad (7)$$

where F_N is the nuclear structure factor in a unit cell for the reflection of interest. Since σ_{NSF} is somewhat lower than its theoretical value due to extinction effects in the nuclear Bragg scattering, the value for $\vec{F}_M$, which is proportional to the moment, is to be taken as an upper limit. It is worthwhile pointing out, however, that it is the change in the raw, as measured, instrumental flipping ratio I^{off}/I^{on} which serves as an immediate indication of the possible formation of a magnetic moment within the sample—if a σ_{SF} appears, I^{off}/I^{on} must decrease, assuming spurious effects remain constant. However, because the magnitudes of the predicted moments are relatively small, the associated magnetic intensity can be orders of magnitude lower than that of nuclear origin which coincides. Thus, the predominant component of I^{on} can be leakage due to imperfect instrumental polarizing efficiency.

Information regarding such experimental details as collimations and particular polarizers used are given along with the corresponding sample and scattering geometry in the tables below wherein specific results are reported. All neutron-scattering measurements at the Center for Neutron Research at NIST were performed on either the SPINS polarized neutron spectrometer or the NG-1 polarized beam reflectometer/diffractometer. The curved stack, Fe/Si supermirror (SM) transmission polarizers which were used are described in Ref. 6. The supermirror transmission polarizers pass predominantly negative spin state neutrons. The presence of a polycrystalline Be filter cooled to liquid-nitrogen temperature efficiently eliminated higher-order wavelength neutrons reflected by the pyrolytic graphite (PG) (002) monochromator. A Heusler (H) (111) crystal in Laue reflection geometry was used as a polarization analyzer for some of the measurements.

B. Neutron polarimetry experiments performed at ILL

The samples of $La_{1.925}Sr_{0.075}CuO_4$ and $YBa_2Cu_3O_{6.7}$ were also examined with the zero-field polarimeter (CRYOPAD) at the Institut Laue Langevin, Grenoble in France. This instrument has been described by Brown *et al.*[9] and a recent example of a magnetic structure determination is given in Brown and Chattopadhyay.[10] Briefly, the instrument allows three-dimensional polarization analysis to be performed; thus instead of measuring only the projection of the neutron polarization on the axis of quantization, the zero-field polarimeter determines all three components of the outgoing neutron polarization vector, thereby allowing a *vectorial* study of the interactions that take place at the sample position. A key feature of the instrument is that the sample is contained in a Meissner shield so that the field at the sample is strictly zero.

For the present experiments only a limited aspect of the capability of the CRYOPAD is used. The samples were oriented so that the scattering plane contained the (110) and (001) axes (in tetragonal notation). Since the assumed antiferromagnet moment is parallel to *c*, the magnetic interaction vector ($\vec{M}_\perp$) for determining the scattering process will be the projection of this moment direction on the plane perpendicular to the scattering vector; $\vec{Q}$. $\vec{M}_\perp = 0$ for reflections of the form $(00L)$, as expected, but for $(HH0)$-type reflections $|\vec{M}_\perp| = \mu$ and this component is parallel to the (001) axis. We now consider the three components of the incident polarization $\vec{P}^i$. For convenience these can be defined in the crystal coordinate system as $P_x = \vec{P}^i // (110), P_y = \vec{P}^i // (001)$, and $P_z = \vec{P}^i // (1\bar{1}0)$.

We may derive the final polarization $\vec{P}^f$ of a beam of neutrons with incident polarization $\vec{P}^i$. Assuming that $\vec{M}_\perp$ is small and has inversion symmetry, a component of the final polarization perpendicular to $\vec{P}^i$ will be proportional to the ratio of $|\vec{M}_\perp|$ to the nuclear structure factor $|F_N|$ for a given reflection (hkl).[9] This perpendicular component is zero when $\vec{P}^i$ and $\vec{M}_\perp$ are parallel. In effect, whatever the value of $|\vec{M}_\perp|$ is, no rotation of the polarization will be expected when $\vec{M}_\perp$ and $\vec{P}^i$ are parallel. In our case this corresponds to $\vec{P}^i = P_y$. For incident polarization P_x and P_z, right-handed orbital currents (with respect to the local oxygen environment) will rotate the polarization one way and left-handed currents will rotate the polarization in the opposite sense. Since these are equally likely, the expected result is a *depolarization* in both the P_x and P_z channels, which should be equal, and proportional to the quantity $|\vec{M}_\perp|/|F_N|$. It can be shown quite simply that the resultant depolarization $\Delta P \sim \gamma/2$ where $\gamma = |F_M|/|F_N|$ and where $|F_M|$ contains the neutron interaction term and the geometric magnetic structure factor, which in turn is proportional to $|\vec{M}_\perp|$. This approximation is valid in the case of $|F_M| \ll |F_N|$, which is certainly the case here as we are searching for a magnetic moment of less than $0.1\mu_B$.

The experiment consists of observing the Bragg peak at a given temperature and then measuring consecutively the polarization in all six directions, $(\pm P_x, \pm P_y, \pm P_z)$. Normally it is necessary to measure a background to subtract from the measured signal, but the count rates from the crystals used were so large compared to the background, that the background measurements were negligible and the crystal was not moved.

Individual values of modulus $\vec{P}^i$, P^i, were about 0.9, which corresponds to a flipping ratio $R = (1+P^i)/(1-P^i) \sim 10$. Higher polarization ($\sim 0.94$) can be obtained with a smaller incident beam, but since the crystals were large (>1.5 cm^2 in cross section) the limiting factor in determining a small depolarization was statistical rather than due to lack of polarization. Individual values of the six polarization components varied by as much as 0.0050, but this is not surprising given the complex rotation of the polarization required to place the neutron polarization in each of the six directions. More importantly, the reproducibility of each operation was found to be limited entirely by the statistics. Thus, over a period of days the stability of a given polarization was better than 0.0002, when exactly the *same* measurement was repeated and sufficient counts accumulated. It is this reproducibility of the CRYOPAD polarization which allowed the very small limits given below to be placed on any orbital current in both the high-T_c materials.

IV. SAMPLE DESCRIPTION AND PREPARATION

A. Bell $La_{2-x}Sr_xCuO_4$ ($x = 0.075$) sample

The first samples studied were underdoped $La_{1.925}Sr_{0.075}CuO_4$ single crystals grown at Bell Laboratories, and henceforth referred to as the ''Bell'' samples. The crystals were grown using the CuO flux method and magnetic susceptibility measurements confirmed that they had a superconducting transition at around 10 K, consistent with this level of doping. Two such crystals with total mass of 1.67 g were aligned together and mounted inside a displex cryostat.

B. Tohoku $La_{2-x}Sr_xCuO_4$ ($x = 0.10$) sample

The starting materials for preparation of the feed and the solvent rods were 4*N* La_2O_3, CuO, and $SrCO_3$. The raw materials were mixed and calcined at ~ 800–$1050\,^\circ$C for 50 h in air with intermediate grindings. The powder was pressed into a cylindrical shape 6 mm in diameter and 120 mm in length under a hydrostatic pressure of about 1700 Kg/cm^2. The rods were sintered at 1100 and $900\,^\circ$C for 12 h in air for the feed and the solvent rods, respectively. Feed and seed shafts were rotated oppositely at a rate of 30 rpm. The zone-traveling rate was 1.0 mm/h. The growth experiments were performed under a gas flow of oxygen.

C. Princeton $YBa_2Cu_3O_{7-x}$ ($x = 0.5$) sample

The YBCO ($x = 0.5$) sample is a single crystal of mass 23.30 g with a $T_c \sim 52$ K. It was grown using top seeded sintering techniques. After oxygenating fully by annealing under pure oxygen, the oxygen is systematically removed by annealing under pure argon until a certain fraction of oxygen remains. The specimen was then sealed in an evacuated quartz tube and annealed for 2 weeks to ensure homogeneity. Superconducting quantum interference device magnetometer measurements of a small piece cut from the sample have been reported elsewhere.[7]

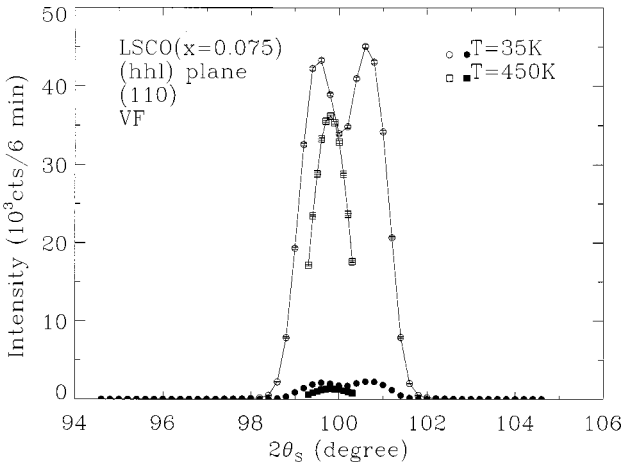

FIG. 5. Longitudinal scan through the (110) peak of LSCO ($x=0.075$) at two temperatures, above and below the structural phase transition. Open symbols are the NSF data and filled ones are the SF data. The sample was mounted such that the (hhl) plane in reciprocal space was the scattering plane (defined by the incident and final neutron wave vectors).

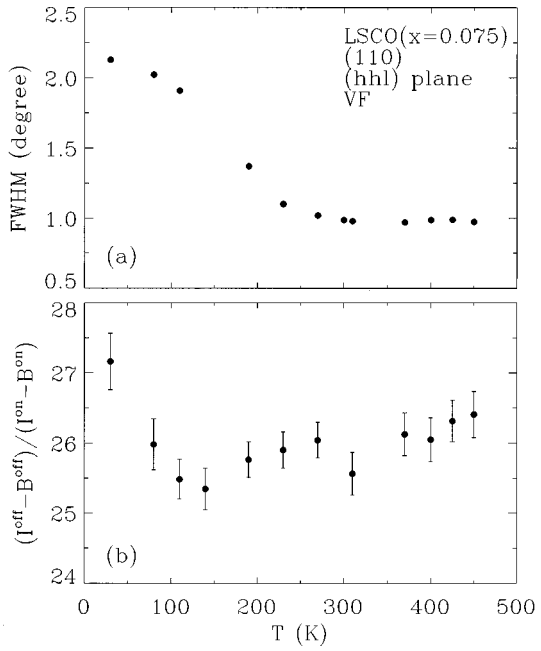

FIG. 6. Temperature dependences (a) of the FWHM of the longitudinal scans and (b) of the flipping ratio, I^{off}/I^{on}, obtained from LSCO ($x=0.075$).

V. RESULTS

A. Conventional polarized neutron diffraction (CPND); Bell $La_{2-x}Sr_xCuO_4$ ($x=0.075$) sample

As already mentioned in a previous section, a structural phase transition occurs over the temperature range of interest for the development of the predicted orbital moment. This is evident in Fig. 5 where the longitudinal peak width of the predominantly structural (110) reflection is split at low temperature (orthorhombic phase) and is about twice as broad, overall, as that at high temperature (tetragonal phase).[8] Although it must be expected that the polarization efficiency or flipping ratio of the instrument can be affected by this intrinsic change in width when convoluted with the imperfect instrumental polarization efficiency distribution, precise and accurate sample alignment and knowledge of the instrumental flipping ratio's dependence on angle allows limits to be placed on the magnitude of moment observable. In this case, for three points about the peak in the longitudinal scan at each temperature, the instrumental flipping efficiency was relatively constant. These three points were summed at each T to produce the raw plot of instrumental flipping ratio versus temperature shown in Fig. 6(b). The specific scattering geometry for these measurements is given in Table I along with the moment calculated by summing low- and high-temperature data sets, respectively. The transverse scan widths in this particular scattering geometry remained approximately constant with temperature. Because the c axis, along which the predicted moments are directed, is perpendicular to the neutron polarization axis, any magnetic contribution to the scattering, obscured by the significantly stronger nuclear scattering associated with the chemical structure, would manifest itself as SF scattering, thereby reducing the observed instrumental flipping ratio I^{off}/I^{on} as discussed in detail above.

The data shown in Fig. 6(b) and Table I suggest the possibility of a weak moment formation at lower temperatures. However, as is evident upon comparison of Fig. 6(a)—for the longitudinal width as a function of temperature—with Fig. 6(b), the structural phase transition and appearance of a moment as indicated by a decreasing flipping ratio appear to be coincident. To obtain definitive evidence for the existence of a moment, better data would have to be obtained. To this end, a second $La_{2-x}Sr_xCuO_4$ sample (with $x=0.10$) (the ''Tohoku'' crystal) was obtained and examined because of its substantially larger volume and resultant higher scattered neutron intensities.

B. CPND; Tohoku $La_{2-x}Sr_xCuO_4$ ($x=0.10$) sample

Because of the occurrence of the structural phase transition in this system, as discussed above, measurements were performed in four different scattering geometries; with the c axis parallel to the scattering plane (hhl) and either parallel or perpendicular to the neutron polarization axis (defined by a magnetic guide field at the sample position of approximate magnitude 40 or 5 Oe, respectively); and with the c axis perpendicular to the scattering plane $(hk0)$ and either parallel or perpendicular to the neutron polarization axis (sample magnetic field 5 or 40 Oe, respectively). All four of these sets of measurements were done for the (110) reflection as a function of temperature. Recall from the discussion of Sec. III that moments directed along the c axis will produce purely spin-flip (SF) scattering if the c axis is perpendicular to the neutron polarization $\vec{P}$.

1. (hhl) scattering plane

Consider first the geometry where the c axis is parallel to the (hhl) scattering plane. As already noted, the width of the (110) reflection in a longitudinal scan increases by approximately a factor of 2 at low temperatures due to the structural phase transition. Furthermore, the peak position changes in angle with temperature due to lattice expansion or contraction. However, at a scattering angle of $2\theta=125.0°$, the scat-

TABLE I. Summary for experiments on $La_{2-x}Sr_xCuO_4$ ($x=0.075$). The wavelength of the incident neutrons was $\lambda=4.1$ Å. Spectrometer configuration: PG(002)-Be-20′ Soller-Curv. SM.-Curv. SM.-20′ Soller-FLP.-SAM.-FLP.-40′ Soller-H(111)-DET. The angular divergences for the beam collimation are given in minutes of arc (′). The nuclear structure factor $F_{\rm Nucl}$ was estimated for a chemical cell containing four Cu^{2+} ions. The flipping ratio was determined from a summation of intensities for three points about the peak.

Q	$\lvert F_{\rm Nucl}\rvert^2$ (barn)	T (K)	$\vec{P}$	Scattering plane	Scan type	$\Gamma_{\rm FWHM}$ (degree)	Flipping ratio	μf (μ_B)
(110)	84.56	$375<T<450$	$[1\bar{1}0]$	(hhl)	$[hh0]$	0.5	26.25(15)	N/A
(110)	84.56	$25<T<150$	$[1\bar{1}0]$	(hhl)	$[hh0]$	1.1	25.99(15)	0.04(2)

tered intensity is well within the full width at half maximum (FWHM) over the temperature range covered as seen in Fig. 7(a): this is of significant advantage since at a fixed scattering angle both instrument and sample magnetic guide fields are stationary and, therefore, constant, irrespective of sample temperature, so that the inherent instrumental polarizing efficiency should remain constant. Transverse scans, as shown in Fig. 7(b), through the (110) position in this geometry had FWHM's which were also nearly constant at all temperatures for both $\vec{P}$ parallel (horizontal field, HF) and perpendicular (vertical field, VF) to the scattering plane [see Fig. 9(a) as well]. The instrumental flipping ratio $I^{\rm off}/I^{\rm on}$ was determined to be $\sim 43(1)$ within about ± 0.03 degree of the peak position in the transverse scan again both for $\vec{P}$ parallel and perpendicular to the scattering plane as shown in Fig. 8. Thus, the instrumental variations in the polarizing efficiency which could have affected the results of the longitudinal scans (where both sample and scattering angles change as a function of temperature) obtained for the Bell $La_{2-x}Sr_xCuO_4$ ($x=0.075$) sample, discussed in Sec. V A, may be reduced by keeping the scattering angle fixed. Nevertheless, the fact that the reflection position, shape, and width are still changing with temperature along the longitudinal direction, when convoluted with the instrumental resolution, may still produce spurious effects on the measured flipping ratios.

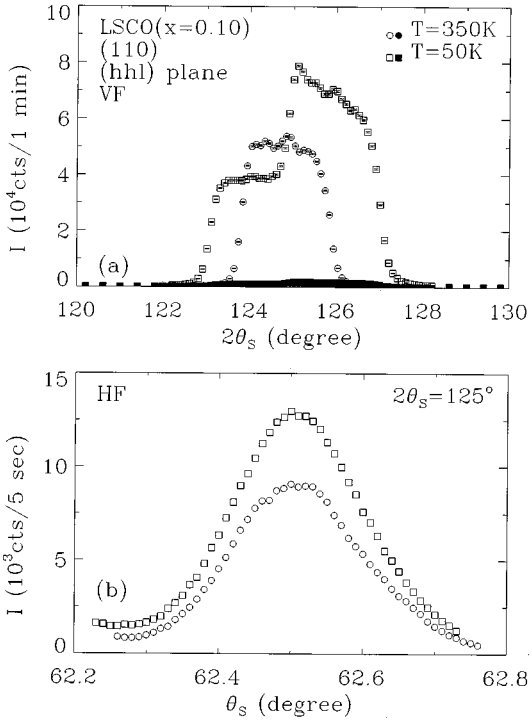

FIG. 7. (a) Longitudinal scans and (b) transverse scans through the (110) peak of LSCO ($x=0.10$) at two temperatures, above and below the structural phase transition. Open symbols are the NSF data and filled ones are the SF data. The sample was mounted such that the (hhl) plane in reciprocal space was the scattering plane.

In Fig. 9(b) is shown the sum of the three highest points in a transverse scan through the (110) reflection versus temperature for both neutron polarization parallel and perpendicular to the scattering plane at a fixed scattering angle $2\theta=125.0°$. In neither case is there a systematic temperature-dependent behavior indicative of the formation of magnetic moment at low temperatures (as would be manifest by a *reduced* flipping ratio at *lower* temperature) within the statistical uncertainties. A similar set of data were obtained at a scattering angle of $2\theta=126.0°$ with essentially the same result. In order to obtain a more quantitative evaluation, the data of Fig. 9(b) (at $2\theta=125.0°$) were combined over two distinct temperature ranges: a lower range from 50 to 200 K inclusive and a higher one from 300 to 400 K. The results of this analysis are presented in Table II which shows that a *negative* value ($-0.052\mu_B$) is obtained for a moment at *lower* temperatures from the data corresponding to the sample c axis, or predicted moment direction, perpendicular to the neutron polarization $\vec{P}$. Within the experimental *statistical* uncertainty of $\pm 0.007\mu_B$, no moment has been ob-

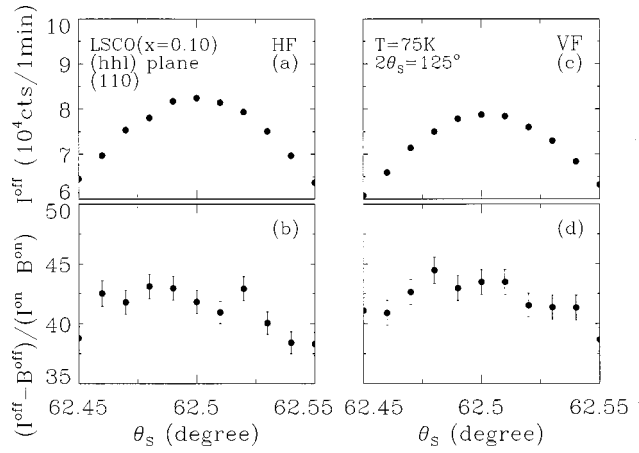

FIG. 8. Transverse scans through the (110) reflection and their flipping ratios (a,b) for horizontal guide field (HF) ($\vec{P}\|\vec{c}$) and (c,d) for vertical guide field (VF) ($\vec{P}\perp\vec{c}$).

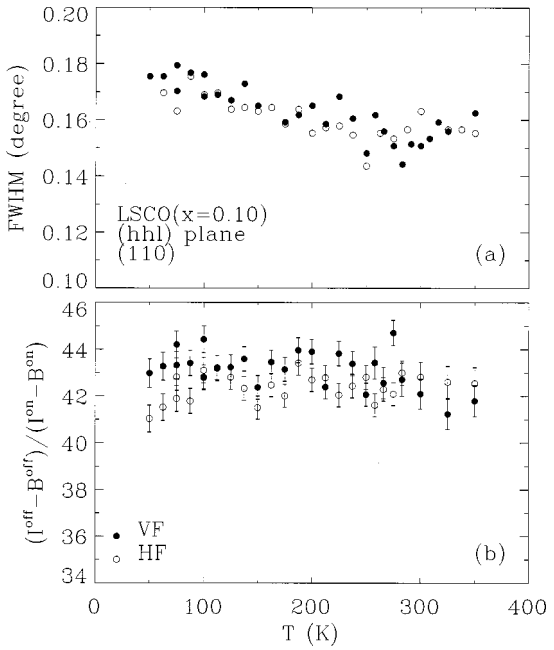

FIG. 9. Temperature dependences (a) of the FWHM of the transverse scans and (b) of the flipping ratio, I^{off}/I^{on}, obtained for LSCO ($x=0.10$).

served. However, the fact that a *negative* value was obtained can be interpreted as an indication of a *systematic* instrumental uncertainty since only either a positive value or zero is expected. Thus, the effective uncertainty for this particular measurement could be taken to be $\pm 0.05\mu_B$. Note that for the geometry in which the c axis is parallel to $\vec{P}$, a moment along the c axis would not give rise to SF scattering: from Table II it can be seen that here the instrumental flipping ratios at low- and high-temperature ranges are almost identical.

2. $(hk0)$ *scattering plane*

Suppose that the predicted orbital moments are correlated much more strongly within the (a,b) plane than perpendicular to it. Then the scattering expected at the (110) point in reciprocal space for a three-dimensional structure will become an extended rod through (110) and parallel to the c axis. In this case the magnetic scattering intensity would be significantly spread out from a point to that approaching a line, depending upon the degree of correlation. In order to increase the possibility of observing such a magnetic rod, the c axis of the sample can be oriented perpendicular to the scattering plane where the larger vertical angular divergence of the beam ($\sim 2.4°$) results in an elongated resolution ellipsoid along the vertical axis, perpendicular to the scattering plane. Thus, this geometry more efficiently integrates any scattering spread out along the perpendicular to the scattering plane.

There is, however, a disadvantage associated with this scattering geometry. The transverse scans through the (110) position will be broadened by the structural phase transition and, as will be illustrated below, this will have a detrimental effect on the instrumental polarizing efficiency: as the transverse width increases at low temperature, the instrumental flipping ratio will decrease. It is, therefore, essential to compare data for the c axis perpendicular to the neutron polarization $\vec{P}$ (where magnetic moments collinear with the c axis would give rise to spin-flip scattering) with that in which the c axis is parallel to $\vec{P}$. For the c axis parallel to $\vec{P}$, an additional complication may arise, which has not yet been discussed, involving the effect of a magnetic-scattering component in the non-spin-flip (NSF) channel which would primarily contribute to I^{off}. However, as will be discussed in detail below, the effect alluded to here requires a particular magnetic domain configuration and can be distinguished experimentally by proper analysis of the measured spin-dependent intensities.

Figure 10(a) shows representative longitudinal scans through (110) at low and high temperatures. However, in contrast to the relatively constant transverse scan widths for the (hhl) (or c axis parallel to the scattering plane) geometry, in the $(hk0)$ orientation the transverse scan width through (110) changes markedly with temperature, as illustrated in Figs. 10(b) and 13(a). Unfortunately, this change in transverse width as a function of temperature due to the structural phase transition significantly affects the angular dependence of the instrumental polarizing efficiency as is evident in the plot of flipping ratio versus angle shown in Fig. 11 at high and low temperature.

Figure 12 shows the flipping ratios measured at each scattering angle position 2θ at a given temperature for the neutron polarization $\vec{P}$ both parallel and perpendicular to the c axis. A transverse scan was performed at each 2θ setting to obtain consistent and optimum alignment (maximum intensity) in order to minimize the effects of the varying angular width on the instrumental polarization. Although the flipping ratio is seen to be relatively constant with scattering angle

TABLE II. Summary for first set of experiments on $La_{2-x}Sr_xCuO_4$ ($x=0.10$). The incident neutron wavelength was $\lambda=4.75$ Å. Spectrometer configuration: PG(002)-Slit-Flat SM.-Curv. SM.-Slit (14′)-FLP.-SAM.-10′ Soller -Curv. SM.-Slit-Flat SM.-Slit (48′)-Be-DET. The flipping ratio was determined from a summation of intensities for three points about the peak.

Q	$\lvert F_{Nucl}\rvert^2$ (barn)	T (K)	$\vec{P}$	Scattering plane	Scan type	Γ_{FWHM} (degree)	Flipping ratio	μf (μ_B)
(110)	84.56	$300<T<400$	[001]	(hhl)	$[00l]$	0.22(2)	42.44(30)	N/A
(110)	84.56	$50<T<200$	[001]	(hhl)	$[00l]$	0.21(2)	42.36(14)	N/A
(110)	84.56	$300<T<400$	$[1\bar{1}0]$	(hhl)	$[00l]$	0.22(2)	42.30(27)	N/A
(110)	84.56	$50<T<200$	$[1\bar{1}0]$	(hhl)	$[00l]$	0.21(2)	43.38(15)	$-0.052(7)$

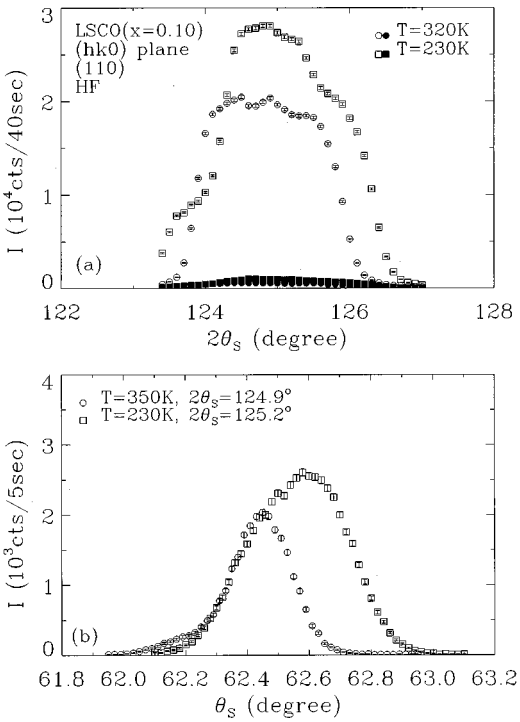

FIG. 10. (a) Longitudinal scans and (b) transverse scans through the (110) peak of LSCO ($x=0.10$) at two temperatures, above and below the structural phase transition. Open symbols are the NSF data and filled ones are the SF data. The sample was mounted such that the $(hk0)$ plane in reciprocal space was the scattering plane.

over a considerable range at any given temperature and for either orientation of $\vec{P}$, it is clear that the low- and high-temperature ranges have a distinctly different average value. Taking the mean flipping ratio, averaged over a range of 2θ where it was uniform to within a few standard deviations, for each temperature, and for both orientations of $\vec{P}$, the plot shown in Fig. 13(b) was constructed. Had only the data corresponding to $\vec{P}$ perpendicular to the c axis [HF for the $(hk0)$ scattering plane with the c axis vertical or perpendicular] shown such a temperature dependence and the other orientation remained flat as indicated by the dashed line in Fig. 13(b), this would be convincing evidence for the formation

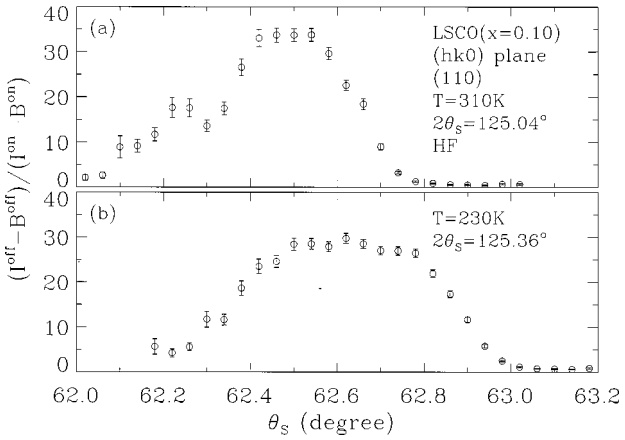

FIG. 11. Flipping ratios obtained from transverse scans at two different temperatures, (a) above and (b) below the structural transition temperature.

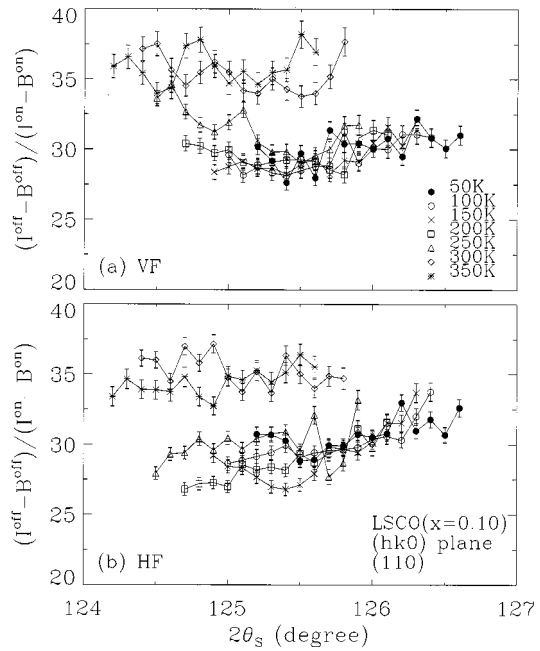

FIG. 12. Flipping ratios measured for LSCO ($x=0.10$) at each scattering angle 2θ at a given temperature for (a) $\vec{P}\|\vec{c}$ and (b) $\vec{P}\perp\vec{c}$.

of a moment along the c axis at low temperatures. However, the nearly identical results obtained for $\vec{P}$ parallel to the c axis cannot be explained by the postulated antiferromagnetic structure with moments collinear with the c axis.

Ignoring this inconsistency for the time being, consider only the data for $\vec{P}$ perpendicular to the c axis in Fig. 13(b). The results of converting only these flipping ratios to a magnetic moment, as discussed in previous sections, gives a value of approximately $0.15\mu_B$. Assume, for the sake of

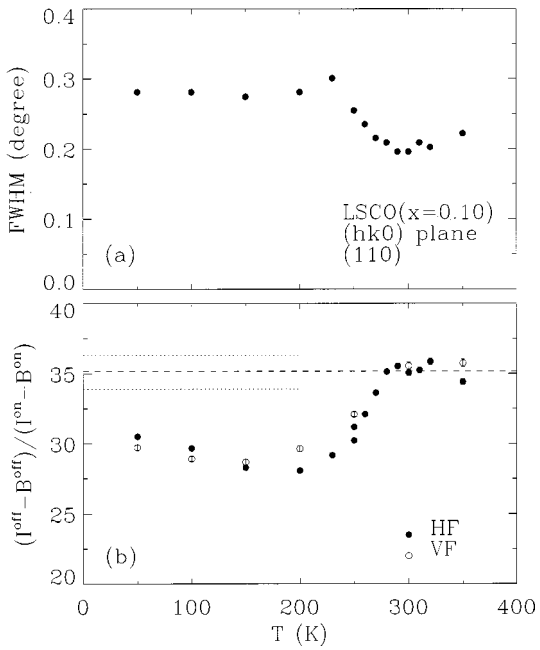

FIG. 13. Temperature dependences (a) of the FWHM of the transverse scan and (b) of the flipping ratio, $I^{\mathrm{off}}/I^{\mathrm{on}}$, obtained for LSCO ($x=0.10$) in the $(hk0)$ scattering plane. The significance of the dotted and dashed lines are discussed in detail in the text.

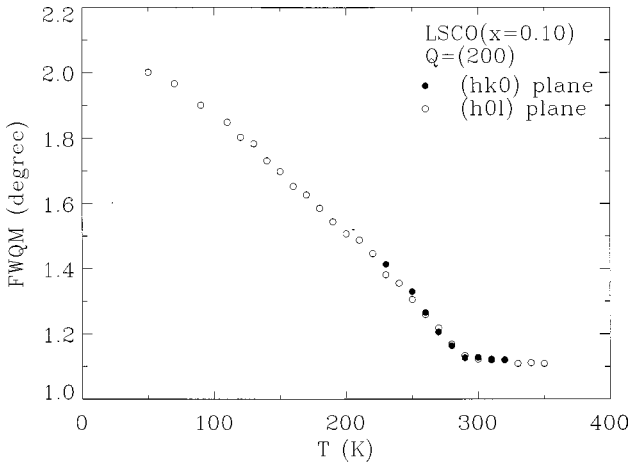

FIG. 14. The temperature dependences of the longitudinal scan widths which reflect the structural phase transition around $T=290$ K.

argument, that this ''moment'' is real and not an artifact due to a systematic degradation of the instrumental polarizing efficiency related to the broadening of the (110) reflection in the transverse direction with decreasing temperature. Is there a way that this $0.15\mu_B$ could explain the nearly equivalent result obtained for $\vec{P}$ parallel to the *c* axis where any moment collinear with the *c* axis could possibly give rise to non-spin-flip scattering (which would primarily contribute to I^{off})? Suppose that the sample constitutes, or is crystallographically equivalent to, a single magnetic domain and that the structure factor is such that the entire $0.15\mu_B$ moment along the *c* axis interferes with the nuclear component (corresponding to the maximum effect). Then the formulas presented in Sec. III would predict, for the flipping ratio,

$$\frac{I^{\text{off}}}{I^{\text{on}}} \simeq 35.1 \cdot \left[1 \pm 2 \left| \frac{\vec{F}_M}{F_N} \right| \right], \tag{8}$$

where the factor 35.1 is the flipping ratio observed at high temperature where the moment is presumed to disappear (the $+$ and $-$ signs correspond to the two possible incident neutron spin states). Substituting the values of F_N and $0.15\mu_B$ gives $I^{\text{off}}/I^{\text{on}} \simeq 36.3$ and 33.9. These values are indicated by the dotted lines shown in Fig. 13(b). Apparently this did not occur (and the smaller the extent of this possible interference, the closer the dotted lines should approach the dashed horizontal line). Furthermore, the longitudinal scan width data shown in Fig. 14 are consistent with the hypothesis that most, if not all, of the observed effect is indeed instrumental and related to the structural phase transition.

Nonetheless, some part of the observed effect may still be due to the formation of the moment. In order to separate a possible genuine moment from the instrumental effect, the data of Fig. 13(b) corresponding to $\vec{P}$ parallel to the *c* axis can be used as a reference, any deviation from which can be ascribed to a possible moment. The average flipping ratio for the points at and below 200 K with $\vec{P}$ parallel to the *c* axis (VF) is 29.23 whereas for $\vec{P}$ perpendicular to the *c* axis an average of 29.14 is obtained. As given in Table III, where the uncertainties listed are larger than the statistical part alone in order to account for systematic fluctuations, the estimated moment is $0.02\mu_B$ but highly uncertain (± 0.08). It should be pointed out that for this particular geometry in which the *c* axis is perpendicular to the scattering plane, the value of integrating any magnetic scattering dispersed along a rod parallel to the *c* axis may be outweighed by the substantial negative effect that the structural phase transition has on the instrumental polarizing efficiency.

Lastly, it must be remarked that a magnetic structure in which the predicted moments were canted 45° relative to the *c* axis would produce equivalent amounts of SF magnetic scattering for either $\vec{P}$ parallel or perpendicular to the *c* axis. For the limited number of reflections accessible at the neutron wavelengths available in these experiments, it was not possible to conclusively establish the existence of such a structure.

C. CPND; Princeton YBCO ($x=0.5$) sample

Given the difficulties associated with the occurrence of the structural phase transition in the $La_{2-x}Sr_xCuO_4$ system, the YBCO sample from Princeton proved to be far less problematic. Not only is the interfering structural phase transition absent, but the nuclear structure factors at the reflections of interest are significantly lower, making the sensitivity to any magnetic moment correspondingly greater. The width of the reflections were nearly constant over the entire temperature range of interest. The results for this system are succinctly summarized in Table IV. A variety of reflections was investigated, including the (110), the (112) (corresponding to a possible ferromagnetic stacking of planes along the *c* axis), and the (002) where no moment should be observed according to the theory, and (111.7) (corresponding to AFM coupling of bilayers). For this system, a sensitivity limit of about $0.03\mu_B$ was obtained, although the average result at the

TABLE III. Summary for second set of experiments on $La_{2-x}Sr_xCuO_4$ ($x=0.10$). The wavelength of the incident neutrons was $\lambda=4.75$ Å. Spectrometer configuration: PG(002)-Slit-Flat SM.-Curv. SM.-Slit (14′)-FLP.-SAM.-20′ Soller -Curv. SM.-Slit-Flat SM.-Slit (48′)-Be-DET. The flipping ratio was determined from a summation of intensities for several points about the peak. Note that in this case, where a comparison is made *not* between high and low temperatures but, rather, between $\vec{P}$ parallel and perpendicular to the *c* axis, the uncertainty quoted is primarily attributed to a systematic rather than statistical variation.

Q	$\lvert F_{\text{Nucl}}\rvert^2$ (barn)	T (K)	$\vec{P}$	Scattering plane	Scan type	Flipping	μf (μ_B)
(110)	84.56	$0<T<200$	[001]	$(hk0)$	$[hh0]$	29.23 ± 1.0	N/A
(110)	84.56	$0<T<200$	$[1\bar{1}0]$	$(hk0)$	$[hh0]$	29.14 ± 1.0	0.02 ± 0.08

TABLE IV. Summary for experiments on $YBa_2Cu_3O_{7-x}$ ($x=0.5$). The wavelength of the incident neutrons was $\lambda=4.005$ Å. Spectrometer configuration: PG(002)-Be FLT-20′ Soller-Curv. SM.-Curv. SM.-40′ Soller-FLP.-SAM.-40′ Soller-H(111)-80′ Soller-DET. The nuclear structure factor F_{Nucl} was estimated for a unit cell containing three Cu^{2+} ions. Some flipping ratios, indicated by an *, were determined from a summation of intensities for several points about the peak; otherwise, the ratios were obtained using integrated intensities.

Q	$\lvert F_{\mathrm{Nucl}}\rvert^2$ (barn)	T (K)	$\vec{P}$	Scattering plane	Scan type	Γ_{FWHM} (Å^{-1})	Flipping ratio	μf (μ_B)
(110)	7.23	500	$[1\bar{1}0]$	(hhl)	$[hh0]$	0.0181	23.32(7)	N/A
(110)	7.23	180	$[1\bar{1}0]$	(hhl)	$[hh0]$	0.0171	23.64(6)	−0.030(5)
(110)	7.23	500	$[1\bar{1}0]$	(hhl)	$[hh0]$	0.0181	26.60(14)*	N/A
(110)	7.23	180	$[1\bar{1}0]$	(hhl)	$[hh0]$	0.0171	27.09(12)*	−0.032(6)
(110)	7.23	500	$[1\bar{1}0]$	(hhl)	$[00l]$	0.104	27.29(13)	N/A
(110)	7.23	180	$[1\bar{1}0]$	(hhl)	$[00l]$	0.099	27.11(7)	0.019(9)
(110)	7.23	500	$[1\bar{1}0]$	(hhl)	$[00l]$	0.104	26.74(23)*	N/A
(110)	7.23	180	$[1\bar{1}0]$	(hhl)	$[00l]$	0.099	26.80(12)*	−0.012(26)
(110)	7.23	500	$[1\bar{1}0]$	(hhl)	$[00l]$	0.104	25.16(13)	N/A
(110)	7.23	100	$[1\bar{1}0]$	(hhl)	$[00l]$	0.096	26.01(12)	−0.045(5)
(110)	7.23	500	$[1\bar{1}0]$	(hhl)	$[hh0]$	0.016	29.68(16)	N/A
(110)	7.23	100	$[1\bar{1}0]$	(hhl)	$[hh0]$	0.015	30.38(16)	−0.035(6)
(111.7)	7.23×0.00237[a]	500	$[1\bar{1}0]$	(hhl)	$[hh0]$	0.0406	15.6(25)	N/A
(111.7)	7.23×0.00237[a]	180	$[1\bar{1}0]$	(hhl)	$[hh0]$	0.0423	11.2(12)	0.010(3)
(002)[b]	0.426	500	$[1\bar{1}0]$	(hhl)	$[00l]$	0.015	22.65(23)	N/A
(002)	0.426	180	$[1\bar{1}0]$	(hhl)	$[00l]$	0.015	22.56(22)	N/A
(002)	0.426	500	$[1\bar{1}0]$	(hhl)	$[hh0]$	0.042	25.24(27)	N/A
(002)	0.426	180	$[1\bar{1}0]$	(hhl)	$[hh0]$	0.042	24.90(26)	N/A
(112)	0.471	500	$[1\bar{1}0]$	(hhl)	$[hh0]$	0.028	23.10(29)	N/A
(112)	0.471	100	$[1\bar{1}0]$	(hhl)	$[hh0]$	0.030	25.30(20)	−0.020(3)
(112)	0.471	500	$[1\bar{1}0]$	(hhl)	$[00l]$	0.026	23.85(41)	N/A
(112)	0.471	100	$[1\bar{1}0]$	(hhl)	$[00l]$	0.035	25.14(28)	−0.015(6)

[a]This (111.7) reflection is forbidden for the chemical structure. Since nonzero intensity was observed at this position, F_{Nucl} for this location was taken to be $F_{\mathrm{Nucl}}(111.7)=F_{\mathrm{Nucl}}(110)\cdot I^{\mathrm{off}}_{(111.7)}/I^{\mathrm{off}}_{(110)}$.
[b]No moment is expected at the (002) reflection.

(110) reflection was $-0.02\mu_B$ (i.e., a negative result implying less moment at temperatures below the predicted magnetic transition than above).

D. CRYOPAD experiments

Using the CRYOPAD technique explained in Sec. III B, we have investigated the LSCO ($x=0.15$) and YBCO ($x=0.7$). At a given temperature and reflection we defined two quantities of interest: the overall average polarization $\langle P\rangle$ of the scattered beam, and the internal depolarization $\Delta P=[P_y-(P_x+P_z)/2]$. For each P^i two measurements are taken, $\pm P^i$, and the average is used. Recall that this quantity ΔP should represent the detection of any orbital current as the latter should affect the P_x and P_z components (as explained above), but not the P_y component. The results are given in the Table V. One can see that the polarization $\langle P\rangle$ changes both for different reflections and also as a function of temperature. The latter is particularly marked in the $(La,Sr)_2CuO_4$ sample, which has a structural distortion, and the mosaic structure of the (110) reflection was quite different as a function of temperature. This value of $\Delta\langle P\rangle=\langle P\rangle_{\mathrm{HT}}-\langle P\rangle_{\mathrm{LT}}$ is significantly greater than any internal ΔP and would indicate a considerable value ($\sim 0.16\mu_B$) for the orbital current—if it was correct. However, the internal difference of polarization ΔP as measured by the CRYOPAD is $(11\pm 3)\times 10^{-4}$ for this reflection in the LSCO, which is almost an order of magnitude smaller. Initially we were optimistic that this possible nonzero value was significant; however, the measurements at 490 K, when the orbital current should be zero, gave the same ΔP, thus showing conclusively that this small number was related to the instrument and the real ΔP can be estimated as less than 5×10^{-4} for the (110) reflection for the LSCO sample. The actual values of ΔP are interesting in that they are clearly distributed not around zero, as would be expected for a perfect instrument, but around some small positive number $\sim 5\times 10^{-4}$. Since this is independent of (hkl) reflection, sample or temperature, we suspect that it is a systematic effect in the instrumental set up. The magnetic structure factor for the orbital current contribution to the (002) for the LSCO and for the

TABLE V. Results for the CRYOPAD experiments on two high-T_c materials. The reflection indices are given in the high-temperature tetragonal notation. The average polarization for the six channels is $\langle P\rangle$, with the difference between the high- and low-temperature values being given by the final column. The quantity ΔP is defined in Eq. (8) and is a true measure—*at a given temperature*—of any possible orbital current.

Material	T (K)	Q (hkl)	$\langle P\rangle$	$(\times 10^4)\Delta P$	$10^4(\langle P\rangle_{HT}-\langle P\rangle_{LT})$	$(\mu f)_{max}$ (μ_B)
$La_{1.925}Sr_{0.075}CuO_4$	50	(002)	0.9110(3)	5 ± 4		N/A
	50	(110)	0.8991(3)	10 ± 3	$+(92\pm4)$	0.009
	490	(110)	0.9083(3)	11 ± 3		N/A
$YBa_2Cu_3O_{6.7}$	300	(200)	0.8664(2)	0 ± 2		N/A
	300	(110)	0.8884(3)	7 ± 2		N/A
	100	(110)	0.8908(3)	7 ± 3	$-(22\pm4)$	-0.004
	300	(112)	0.8760(4)	4 ± 6		N/A
	100	(112)	0.8809(4)	7 ± 8	$-(49\pm6)$	-0.003

(200) YBCO are zero, so that no effect should be observed, as is experimentally the case. For the $YBa_2Cu_3O_{6.7}$ sample the overall average polarizations were lower because of the larger crystal (~ 3 cm^2 cross section area and ~ 1 cm thick), and there seems to be a small improvement in $\langle P\rangle$ at low temperature. However, the internal ΔP shows that any effect is also less than 5×10^{-4}. In the case of the (112) the statistical uncertainty is about 8 in these units as the reflection is weaker. As explained above in the limit of $|F_M| \ll |F_N|$ the $\Delta P \sim 0.5|F_M|/|F_N|$. If we normalize the structure factors to a single Cu atom, F'_N, then $\gamma = 0.27\mu f/|F'_N|$ where μf is the product of the moment and the form factor of any orbital current directed along the c axis. Rearranging gives

$$|\mu f| < 7.4\Delta P|F'_N|. \tag{9}$$

The results are listed in Table V. The negative moments for the YBCO sample indicate that the sensitivity of our YBCO measurements was $0.004\mu_B$ and the upper limit for any orbital moment in the LSCO ($x=0.15$) sample is obtained to be $0.009\mu_B$.

E. Specific search for a magnetic rod

Except for the attempt to increase sensitivity to the possible presence of a magnetic rod described in Sec. V B 2, we have thus far concentrated on three-dimensional ordering of the orbital moments. If the orbital moments order two-dimensionally on the Cu-O plane, the neutron-scattering cross section from the moments would be spread out along the c^* axis which is perpendicular to the Cu-O plane. If the total amount of scattering due to the ordered moment μ is spread over the first Brillouin zone of dimension L_{BZ} along the c^* axis and the full width at half maximum (FWHM) of the Q resolution ellipsoid is ΔQ, then the amount of the moment detected within the Q-resolution window of the instrument would be significantly decreased to $\mu(\Delta Q/L_{BZ})$. One advantage is, however, that in order to measure such a magnetic rod we do not have to do so at the strong nuclear Bragg reflection. Instead, we can move away from the nuclear reflection along the magnetic rod to a position (hhl) which would increase the sensitivity of the measurements. We can not go arbitrarily far away from the (110) reflection because the magnetic scattering along the c^* axis would be $I_{SF}\propto|F_M|^2-|\hat{Q}\cdot F_M|^2=|F_M|^2[1-(lc^*)^2/2(ha^*)^2+(lc^*)^2]$ which decreases as l increases.

We first utilized a horizontally focusing analyzer to relax the instrumental Q resolution along the c-axis direction, and with the unpolarized beam searched for a magnetic rod in YBCO. Unfortunately, the nuclear scattering from the tails of neighboring Bragg reflections was prohibitively high.

Next, we performed polarized neutron-diffraction measurements with tighter collimation and scanned along the direction perpendicular to the rod at a Q where the tail of the strong nuclear reflection is so small that nuclear contamination in the SF process is insignificant. The LSCO ($x=0.1$) sample, which has the narrowest mosaic distribution of all the samples investigated, was selected for the experiment. The measurements were performed at (1,1,0.6) at which the factor, $1-(lc^*)^2/2(ha^*)^2+(lc^*)^2=0.985$ is close to 1. The scattering cross section for the SF process, σ_{SF} was determined using Eq. (5) with the background-subtracted integrated intensities, I_{off} and I_{on}, at different temperatures. As shown in Fig. 15, I_{SF} does not change with temperature and, furthermore, it is negative at all temperatures, indicating

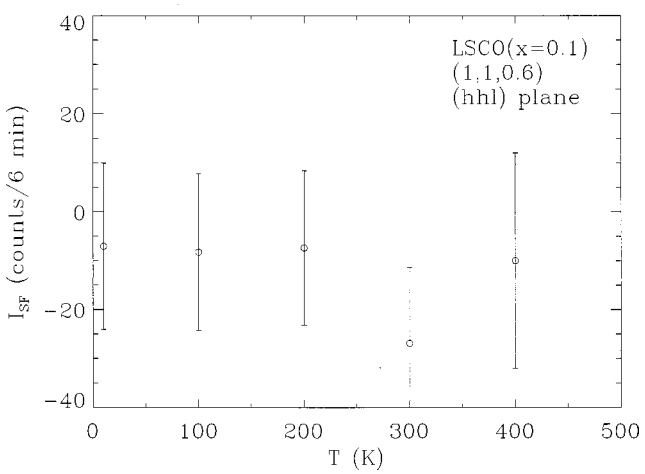

FIG. 15. The temperature dependence of the SF scattering cross section at (1,1,0.6) in LSCO ($x=0.1$).

TABLE VI. Summary for experiments on $La_{2-x}Sr_xCuO_4$ ($x=0.1$) in search of a magnetic rod along the *c*-axis direction. The wavelength of the incident neutrons was $\lambda=4.1$ Å. Spectrometer configuration: PG(002)-Be-Curv. SM.-20′ Soller-SAM.-FLP.-Curv. SM.-20′ Soller-PG(002)-DET. The angular divergences for the beam collimation are given in minutes of arc (′). The measurements were performed at (1,1,0.6), and the full width at half maximum (FWHM) of the instrumental *Q*-resolution ellipsoid was 0.015 $Å^{-1}$. The flipping ratio was determined at (110) at each temperature.

Q	T (K)	$\vec{P}$	Scattering plane	Scan type	Flipping ratio	μf (μ_B)
(1,1,0.6)	10	$[1\bar{1}0]$	(hhl)	$[hh0]$	24.12(17)	−0.004(4)
(1,1,0.6)	100	$[1\bar{1}0]$	(hhl)	$[hh0]$	25.66(17)	−0.003(4)
(1,1,0.6)	200	$[1\bar{1}0]$	(hhl)	$[hh0]$	28.40(20)	−0.003(4)
(1,1,0.6)	300	$[1\bar{1}0]$	(hhl)	$[hh0]$	28.63(26)	−0.004(6)
(1,1,0.6)	400	$[1\bar{1}0]$	(hhl)	$[hh0]$	28.38(27)	−0.004(6)

that the formation of two-dimensional orbital moments at (1,1,0.6) was not detectable within the experimental accuracy. The estimated values for the moments are listed in Table VI. The negative value of the estimated moments detected at (1,1,0.6), $-0.004(4)\mu_B$, is a measure of systematic instrumental uncertainty. The total moment, then, can be determined to be $L_{BZ}[-0.004(4)\mu_B]/\Delta Q \sim -0.1(1)\mu_B$ which is the upper limit for any two-dimensional orbital moment in the LSCO ($x=0.1$) sample.

VI. CONCLUSIONS

No convincing evidence was found for the formation of orbital moments in the cuprate metals as predicted by theory, although experimental sensitivity was limited to approximately $0.01\mu_B$ for three-dimensional ordering and $0.1\mu_B$ for the formation of a two-dimensional rod. In the $La_{2-x}Sr_xCuO_4$ compounds, the primary limitation to the sensitivity was intrinsic, related to the crystallographic tetragonal-to-orthorhombic phase transition over the temperature range of interest which affected the constancy of the instrumental polarizing efficiency.

ACKNOWLEDGMENTS

Work at SPINS is based upon activities supported by the National Science Foundation under Agreement No. DMR-9423101. S. K. Sinha acknowledges support by the U.S. Department of Energy, BES-Materials Science, under Contract No. W-31-109-ENG-38. C. Stassis acknowledges support by the U.S. Department of Energy, BES-Materials Science, under Contract No. W-7405-Eng-82. The authors acknowledge helpful discussions with Dr. G. Shirane and Dr. C. Varma.

[1] A. G. Loeser *et al.*, Science **273**, 325 (1996); H. Ding *et al.*, Phys. Rev. Lett. **78**, 2628 (1997), and references therein.
[2] C. M. Varma, Phys. Rev. B **55**, 14 554 (1997).
[3] G. E. Bacon, *Neutron Diffraction* (Clarendon, Oxford, 1975); S. W. Lovesey, *Theory of Neutron Scattering from Condensed Matter* (Clarendon, Oxford, 1984).
[4] R. M. Moon, T. Riste, and W. C. Koehler, Phys. Rev. **181**, 920 (1969).
[5] C. F. Majkrzak, Physica B **221**, 342 (1996).
[6] C. F. Majkrzak *et al.*, Proc. SPIE **1738**, 90 (1992); C. F. Majkrzak, Physica B **213&214**, 904 (1995).
[7] H. F. Fong, B. Keimer, D. L. Milius, and I. A. Aksay, Phys. Rev. Lett. **78**, 713 (1997).
[8] The splitting of the (110) reflection occurs due to the formation of different domains (where the lattice parameters *a* and *b* are not equal) orthogonal to one another.
[9] P. J. Brown, J. B. Forsyth, and F. Tasset, Proc. R. Soc. London, Ser. A **442**, 147 (1993).
[10] P. J. Brown and T. Chattopadhyay, J. Phys.: Condens. Matter **9**, 9167 (1997).